Supporting Information for

Placental Transport and Metabolism Monitored by Hyperpolarized Dynamic ^{13}C Magnetic Resonance

Stefan Markovic[1†], Anne Fages[1†], Tangi Roussel[1], Ron Hadas[2], Alexander Brandis[3], Michal Neeman[2], Lucio Frydman[1*]*

Supporting Information 1. Full description of the experimental DNP NMR methods.

Animal handling. All studies were performed on pregnant Wistar rats. For the perfusion of the hyperpolarized (HP) metabolites, animals were anesthetized with 3% isoflurane in 1 L/min of O_2, and the tail vein was cannulated for the intravenous injection. The animal was then placed on a custom-made MRI bed holder either on the side or on supine position; prone positions were conducive to weak HP signals, probably due to circulation problems. During the MRI experiments animals were maintained anesthetized using 1-2% isoflurane in 1 L/min of O_2 through a nasal mask. Respiration was monitored throughout using a monitoring and gating system (SA instrument model 1025) and maintained at 30-40 breaths/min by adjusting the isoflurane level. Experiments were performed up to three times on each rat, with a lag time of at least one day between two experiments on the same animal.

Hyperpolarization. For dissolution DNP, the following protocols were followed. 1) 27 mg of ^{13}C-urea (Cortecnet, Voisins-le-Bretonneux, France) were dissolved in glycerol:D_2O (proportion 7:3) with 15 mM Ox063 trityl radical (GE Healthcare, Little Chalfont, UK) to a concentration of 6.4 M. 2) ^{13}C-labeled cesium bicarbonate was used, obtained as described by Gallagher and colleagues[1] by slowly adding $^{13}CO_2$ (Sigma-Aldrich, Saint-Louis, MO) to an evacuated flask containing CsOH hydrate until neutral pH were reached. 78 mg of Cs-^{13}C-bicarbonate were dissolved in glycerol:D_2O (proportion 3:2) containing 15 mM Ox063 trityl radical to a concentration of 4 M. 3) 21 µL of $^{13}C_1$-pyruvic acid was mixed with 15 mM Ox063 trityl radical. For both urea and bicarbonate samples, gadoteric acid (DOTAREM; Guebert, Roissy, France) was also added to the polarized solutions to a final concentration of 1.5 mM. For performing the hyperpolarization, all samples were cooled down to 1.4 K and hyperpolarized in a 3.35 T Hypersense® polarizer (Oxford Instruments, Abingdon, UK), by irradiating with 100 mW microwave powers at appropriate frequencies as applied by an Elva microwave source operating at 94 GHz. After approximately 180 minutes of irradiation ca. 25% of ^{13}C polarization was achieved; the samples were then rapidly dissolved into 4 mL of: 1) PBS for ^{13}C-urea; 2) PBS containing 0.1 g/L EDTA for ^{13}C-bicarbonate; 3) a buffer containing 60 mM NaOH, 40 mM Trizma-PreSet (pH=7.6), EDTA 0.1 g/L and 0.9% NaCl, for the [1-^{13}C]pyruvic acid. For all cases, solutions had a pH ~7.5 upon injection. For n=3 of the bicarbonate dissolutions, the HP cesium ^{13}C-bicarbonate was passed through an ion column (Chelex 100 Resin, Bio-Rad Laboratories) to exchange the Cs by Na before injecting the dissolved sample, but no significant differences were seen in the final ^{13}C MRI results. 3 mL of the 115 mM HP ^{13}C-urea, the 100 mM HP ^{13}C-bicarbonate or the 80

mM HP [1-^{13}C]pyruvate solutions were injected into the tail vein over a period of ~15s, following which ^{13}C MRI were immediately recorded.

NMR data acquisition. All experiments were conducted at 4.7 T on a Bruker Biospec® MRI scanner running ParaVision 4.1. The magnet is characterized by a 30 cm bore that could easily accommodate the pregnant animals, and a gradient insert with maximum gradient of 40 mT/m. Multislice ^{1}H spin-echo and gradient-echo sequences were used for the anatomical details of the fetoplacental units. Coronal gradient-echo sequence (FLASH) were obtained using a 5 ms *sinc* excitation pulse, a repetition time (TR) of 6.3 ms and an effective echo time (TE) of 615 ms. The slice thicknesses were 1 mm (no slice intersection gap) and 6×6 cm^2 field of views (FOVs) were targeted using a 128×128 k-encoding matrix. Additional coronal T_2-weighted fast spin-echo images (RARE) were recorded using the volume coil with the following parameters: 3 ms *sinc* excitation pulse, TE/TR = 15ms/5000ms, 6×6 cm^2 field of view, slice thickness of 1 mm, 128 × 128 in-plane matrix, RARE factor = 4. Motion artefacts due to the maternal breathing were limited on the RARE images by triggering acquisitions with the respiratory gating system. To obtain these anatomical details over the whole FOV, a ^{1}H volume coil was used for irradiation and a ^{1}H/^{13}C surface coil was used for reception to ensure the right positioning of the surface coil toward the fetuses and other organs of interest (e.g., maternal kidney). Dynamic ^{13}C spectroscopic images (MRSI) were recorded using the cross-coil configuration (^{13}C volume transmit / ^{13}C surface receive), with active decoupling. ^{13}C signals were gathered from either 5 mm thick coronal slices (urea and bicarbonate experiments) or 10 mm slice thick (pyruvate) experiments. FOVs of 5.0x5.0 cm^2 were targeted using a centric phase-encoded matrix of resolution 8x8 (bicarbonate), 10x10 or 12x12 (urea and pyruvate). Small tip-angle slice-selective Gaussian pulses were applied to record free induction decays over a period of 42.6 ms for a TR of 46 ms (urea and bicarbonate) or 68 ms (pyruvate). 256 time domain points per acquisition over a 2.7 kHz spectral bandwidth and 384 spectral data points (119 ppm bandwidth), respectively, were recorded. The ^{13}C MRSI images were reconstructed and quantified using a custom Matlab (The Mathworks Inc., Nantucket, OH, USA) software, applying a 20-40 Hz exponential apodization and zero-filling the spatial resolution of the ^{13}C MRSI by interpolation to 32x32. The analyses of the quantified time series, however, were obtained from the original ^{13}C MRSI working with resolutions of 8x8, 10x10 or 12x12 pixels. When the decay was too short to record more than three images the kinetic fitting resolution was effectively increased by reconstructing interleaved images from consecutively acquired *k*-space data, utilizing a "sliding-window" type approach.

Supporting Information 2. GC-MS analyses of ^{13}C urea enrichment in maternal/fetal organs

3 mL of 115 mM (unpolarized) ^{13}C-urea in PBS were injected in anesthetized pregnant rats (E18). The animals were sacrificed by intravenous injection of sodium pentobarbitone (1 mL of 200 mg/mL) one minute after the end of the ^{13}C-urea injection. The heart stopped pulsing at once, and the maternal blood, maternal kidney and maternal liver were collected immediately, as were placentas, fetal livers

and amniotic fluids. The organs were snap frozen in liquid nitrogen and the blood sample was centrifuged (5000 g, 15 min) to collect serum. Hydrophilic metabolites were collected from the different samples by following a standard $MeOH/H_2O/CHCL_3$ extraction protocol.[2] In brief, these samples were weighted and homogenized after adding 4mL/g of MeOH and 0.85mL/g of H_2O. 4mL/g of $CHCl_3$ and an additional 2 mL/g of H2O were added to the sample and the different phases were separated by centrifugation (1500 g, 20 min) after letting the sample with the solvents for 15 min. The upper phase containing the hydrophilic metabolites, including urea, was collected and dried under vacuum prior to storing at -80°C. GC-MS tests were done on such samples as described in Ref 3. Each sample was dissolved in 100 µL of ethanol, then 22 µL TMP (0.3M solution in ethanol) and 40 µL of 25% HCl were added. The mixture was vortexed, incubated at room temperature for 1 h, and then evaporated in a flow of nitrogen at 30˚C. The residue was then dried in lyophilizer for 1 h, and derivatized with 30 µL of MSTFA at 60˚C for 1 h. The mixtures were transferred to a 2-mL autosampler glass vial with a 100-µl glass insert, in order to analyse by GC-MS on an Agilent 7890A gas chromatograph equipped with split/splitless injector and a LECO Pegasus HT Time-of-Flight Mass Spectrometer (TOFMS). Samples were analyzed in the split mode (100:1) providing linearity for the examined concentrations; injector temperature was set at 280°C. Analytes were separated using Helium as carrier gas at a flow rate of 1.0 mL/min. The thermal gradient started at 70°C, was held at this temperature for 1.5 min, ramped to 150°C at 10°C/min and then ramped to 320°C at 20°C/min and held at 320°C for 3.0 min. Eluents were fragmented in the electron impact mode with an ionization voltage of 70 eV. The MS mass range was 50-650 m/z with an acquisition rate of 20 spectra per second. The ion source chamber was set to 230°C and the detector voltage was 1500V. LECO ChromaTOF software was used for acquisition control and data processing. The [M-15(Me)] ion with 153 m/z for ^{12}C-urea and 154 m/z for ^{13}C-urea was monitored. Correction has been made for ^{13}C-urea determination, considering the contribution of 1 Da from naturally abundant isotopes ^{13}C of TMP, ^{29}Si of MSTFA, and from ^{15}N in non-labeled urea. Here, the [M-15(Me)] fragment $C_6H_9ON_2Si$ provides mass increment of 1 Da (i.e. 154 m/z) with

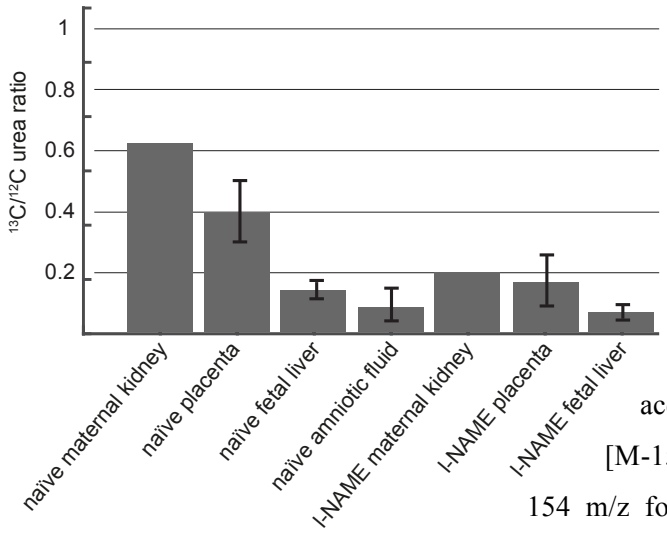

Figure S1. GC-MS measurement of ^{13}C-urea enrichment on metabolic extracts from naïve and l-name treated animals, focusing on maternal kidneys (n=1), placentas (n=5), fetal liver (n=4) and amniotic fluid (n=2). Notice the significant enrichment in ^{13}C-urea revealed by the GC-MS analysis for the fetoplacental units, attesting the urea crossing of the trophoblastic barrier. Notice as well the consistently lower urea values found in these units for the preeclamptic model animals

relative signal intensity 6x1.07+2x0.368+4.6832=11.8392≈12% of the main (153 m/z) signal. Then, the ratio between ^{12}C- and ^{13}C-urea concentrations was calculated from their peak areas as ($A_{13C\text{-}urea}$-$0.12A_{12C\text{-}urea}$)/$A_{12C\text{-}urea}$. Results of these tests for naïve and l-NAME-treated animals are summarized in **Figure S1**

Supporting Information 3. Representative *in vivo* ^{13}C hyperpolarized NMR results obtained for the analyzed metabolites.

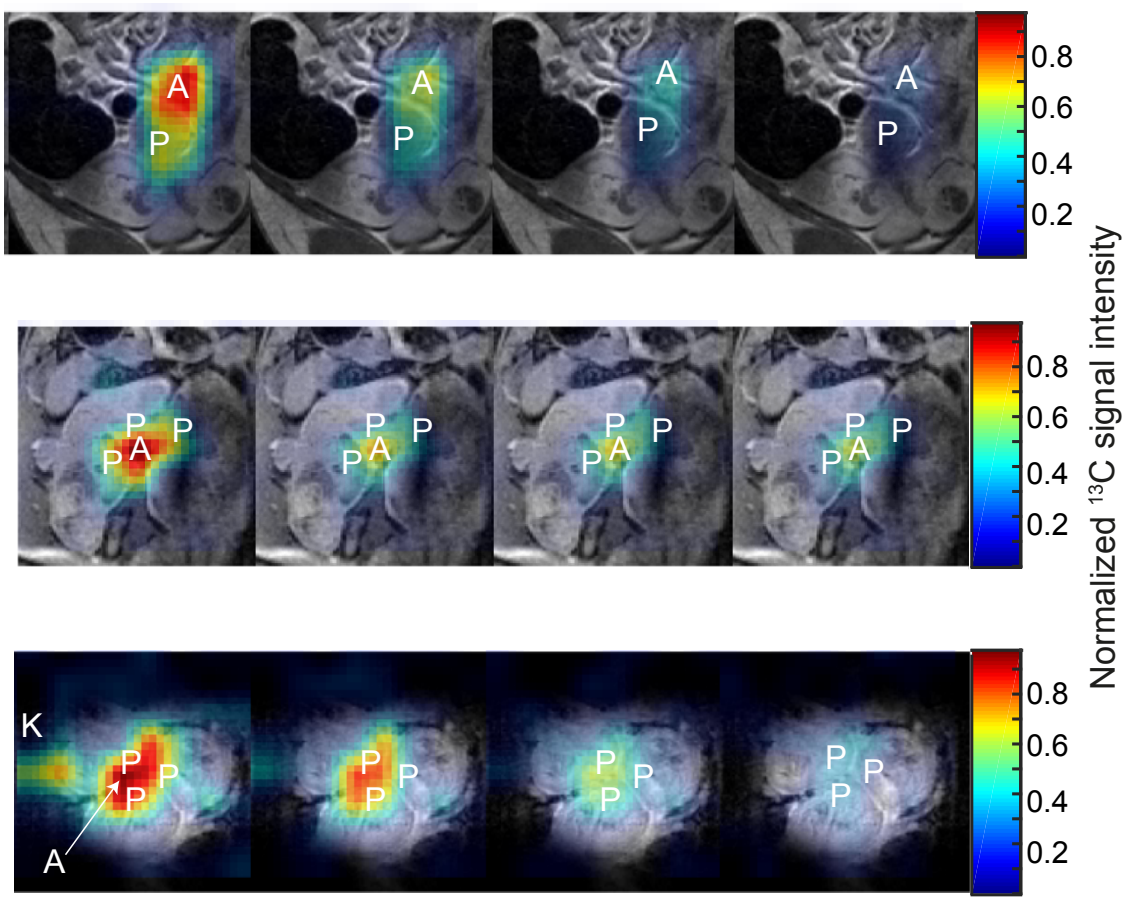

Figure S2. Independent experiments recorded after the injection of HP ^{13}C-labeled cesium bicarbonate, on sidewise-positioned animals. ^{13}C MRI data (1.5x1.5 mm^2 in plane resolution, in color) are overlaid on corresponding ^{1}H MRI slices (grayscale). The most intense HP ^{13}C-bicarbonate signal is generally coming from the maternal artery; signals from placentas are also detectable, and they decay with the same trend as the maternal artery signals. A, maternal artery; P, placenta; K, maternal kidney.

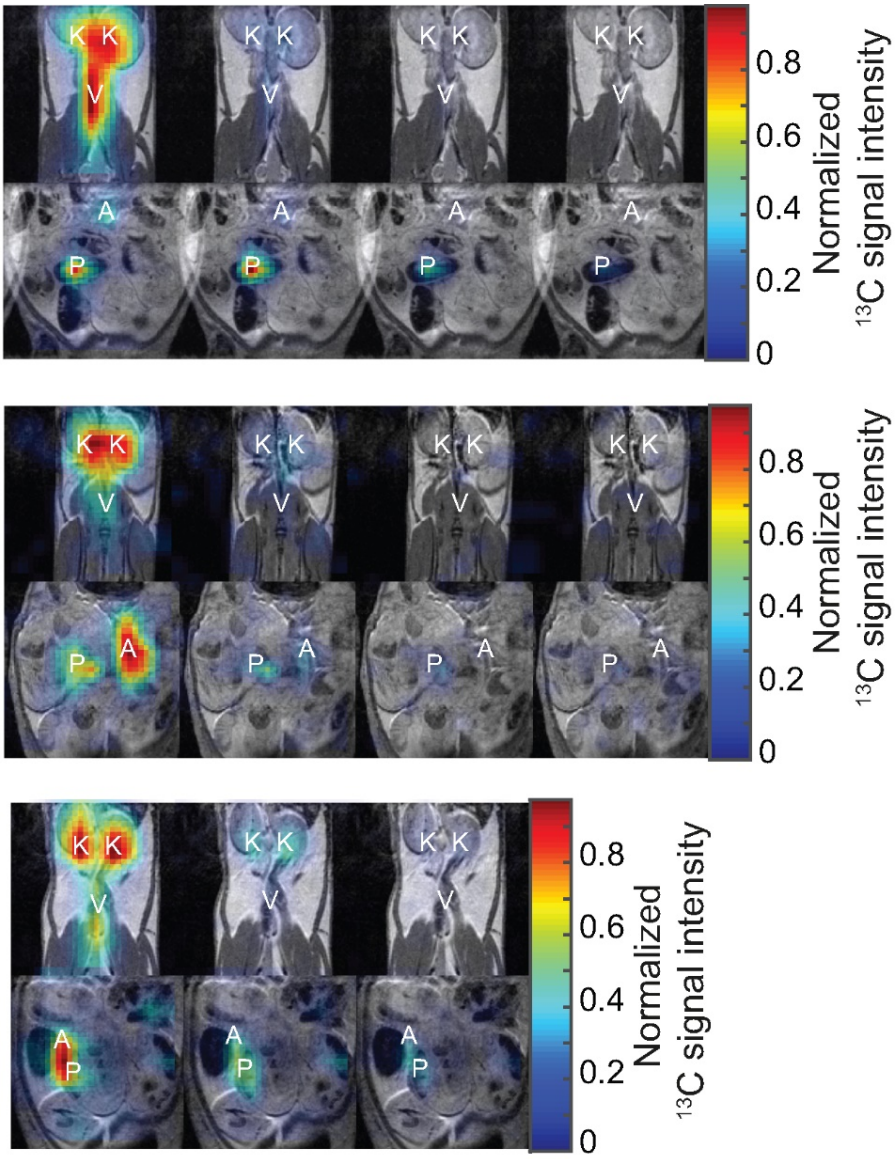

Figure S3. Three ^{13}C MRI experiments recorded after the injection of HP ^{13}C-urea. Dynamic ^{13}C MRSI (1.5x1.5 mm^2 in plane resolution) are shown overlaid on the corresponding ^{1}H MRI slices. The animals were positioned on supine position and ^{13}C images for two-slices, each 5 mm thick, were recorded. The lower slice contains the HP ^{13}C-urea signal from the two maternal kidneys and the vena cava, while signals from the placentas and the maternal uterine artery are detected in the upper slice. Notice the noticeably slower decay of the ^{13}C-urea signal intensity evidenced by the placentas than by the maternal compartments. K, maternal kidney; V, maternal vena cava; A, maternal artery; P, placenta.

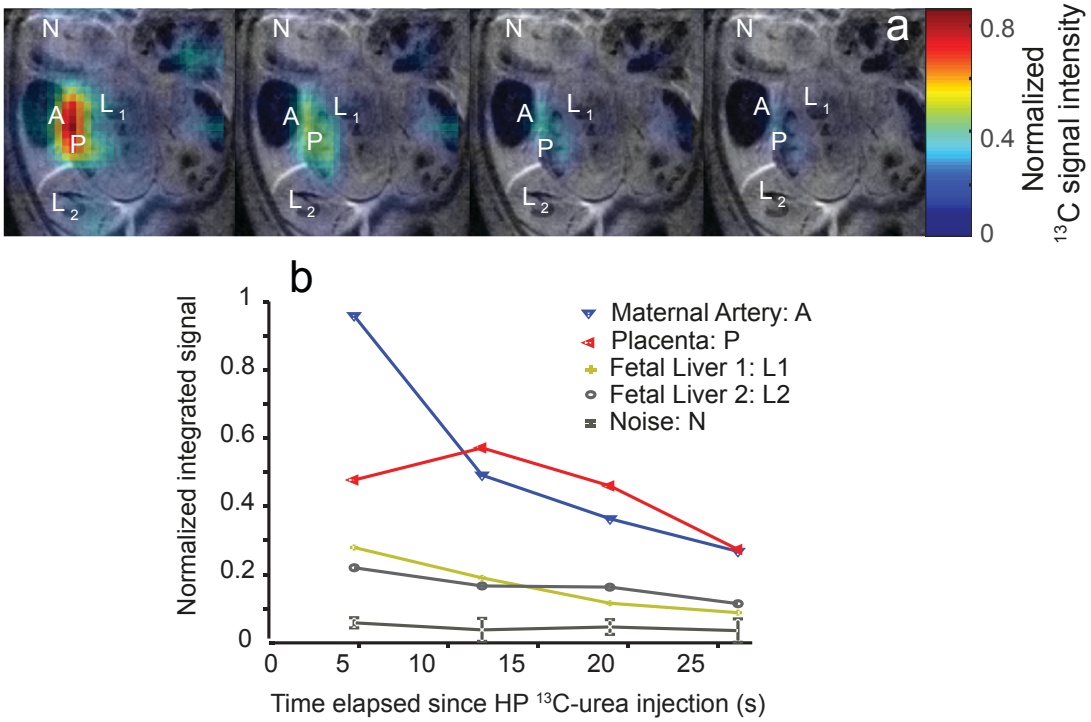

Figure S4. Observation of HP ^{13}C urea inside fetuses by ^{13}C MRI experiments performed on a pregnant rat (E19). (a) Overlaid anatomical and hyperpolarized images collected as a function of time, highlighting signals coming from two different fetal livers with significant signal intensity (5x5 mm^2 in plane resolution, 5 mm slice thickness). (b) Time curves of the ^{13}C-urea signal intensity for relevant pixels.

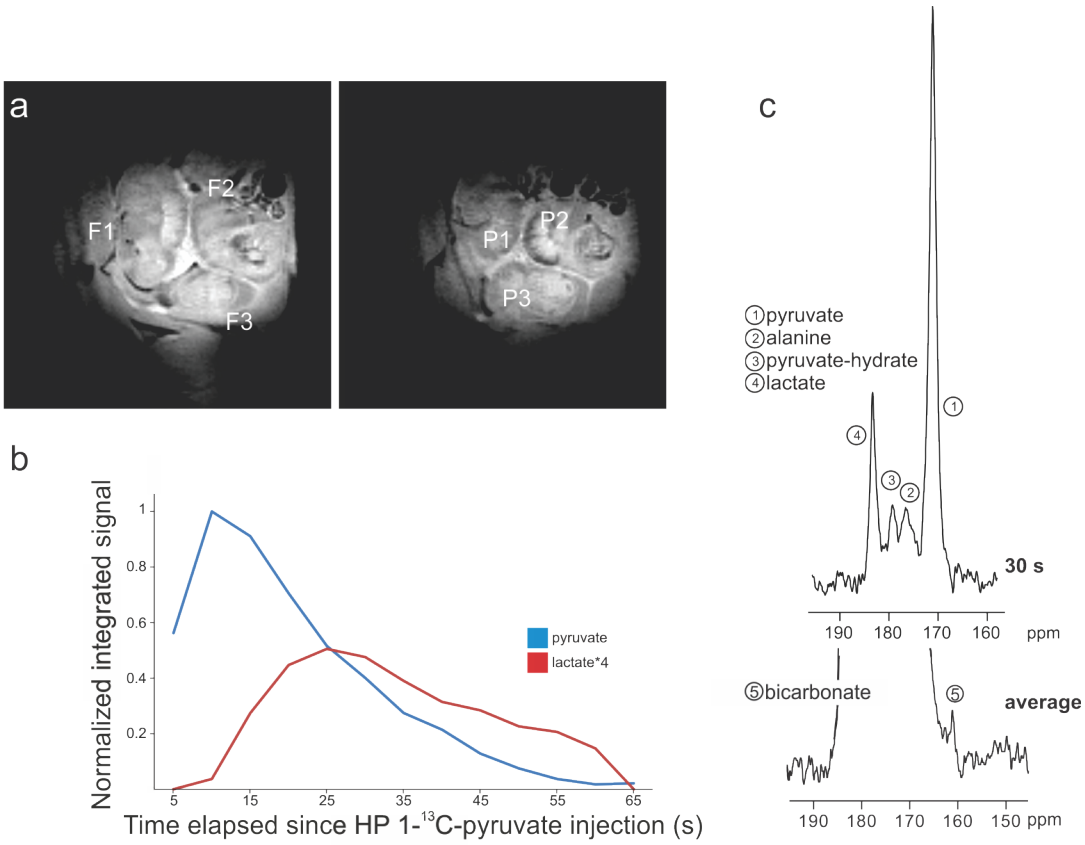

Figure S5. ^{13}C NMR spectra recorded on a pregnant rat (E17) after injection of HP [1-^{13}C]pyruvate. (a) Surface-coil proton FLASH images showing three fetuses (F1, F2, F3) and three placentas (P1, P2, P3) in the detection range of the ^{13}C/^{1}H dual-tuned surface coil used in all experiments. (b) ^{13}C NMR spectral intensities of pyruvate and lactate signals recorded over the field-of-view in (a), with an acquisition time of 0.1 s and a recycle delay of 0.9 s. (c) Top: Representative ^{13}C MR spectrum at ~30 s showing signals for pyruvate, pyruvate-hydrate, alanine and lactate. Bottom: Average of all spectra recorded over 65 s showing as well a bicarbonate signal.

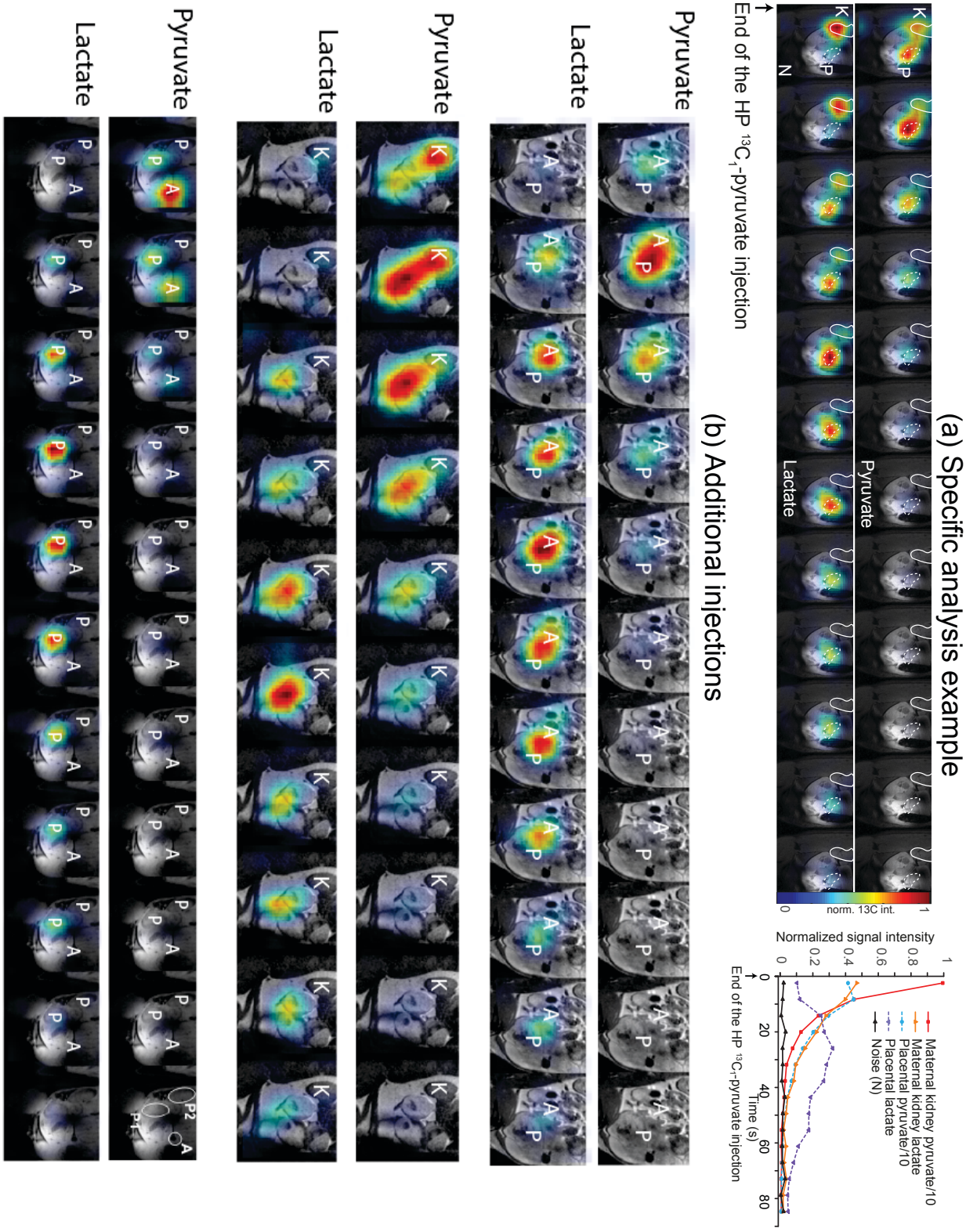

Figure S6. ^{13}C images recorded after the injection of HP [1-^{13}C]pyruvate in four pregnant rats, showing ^{13}C MRSI data recorded after the injection overlaid on the corresponding ^{1}H MRI slices. Upper rows show the HP ^{13}C images arising from [1-^{13}C]pyruvate and the lower rows corresponding images of ^{13}C-lactate. The round continuous region in the top series highlights a maternal kidney and the dashed curves correspond to placentas from different fetuses; the graph on the right of these data shows a typical signal intensity analysis. In all instances ^{13}C MRSI images had 1.5x1.5 mm^2 in-plane resolution and all animals were positioned on their sides to avoid perfusion problems. The ^{13}C time

curves arising from these tests and from that in Figure 4 are further analyzed in Supplement 5. A, maternal artery; K, maternal kidney; P, placenta; N, noise.

Supporting Information 4. Analyses of the hyperpolarized ^{13}C-urea kinetics.

As mentioned in the main text the maternal decay and placental buildup and subsequent decay observed upon injecting HP ^{13}C-urea were modeled according to

$$\frac{d}{dt}U_m = -\frac{U_m}{T_1^{eff}} \;; \qquad \frac{d}{dt}U_p = -\frac{U_p}{T_1^{eff}} + K_{in}\cdot U_m \qquad \text{[S1]}$$

where $U_{m,p}$ reflect the signal intensities of urea in the maternal and placental compartments, T_1^{eff} is an effective signal decay that includes a conventional T_1 contribution, the effect of the pulsing on the nuclear hyperpolarization as well as the washout of the hyperpolarized urea from the maternal vascular system, and K_{in} is a kinetic rate reflecting urea's transport into the placenta. For initial conditions $U_m(0) = U$, $U_p(0) = 0$, these coupled equations yield solutions

$$U_m(t) = U\cdot\exp\left(-\frac{t}{T_1^{eff}}\right);\; U_p(t) = K_{in}U\cdot t\cdot\exp\left(-\frac{t}{T_1^{eff}}\right) \qquad \text{[S2]}$$

The following plots show the best fit of the various experiments carried out in this study to determine the parameters involved in these equations. Some of the parameters derived from these best fits are summarized for each investigated animal in Table S1. In all injections the absolute intensity U (in scanner gain units) vary solely within ±25%, which is remarkable given the polarization, relaxation, injection and perfusion variability between experiments.

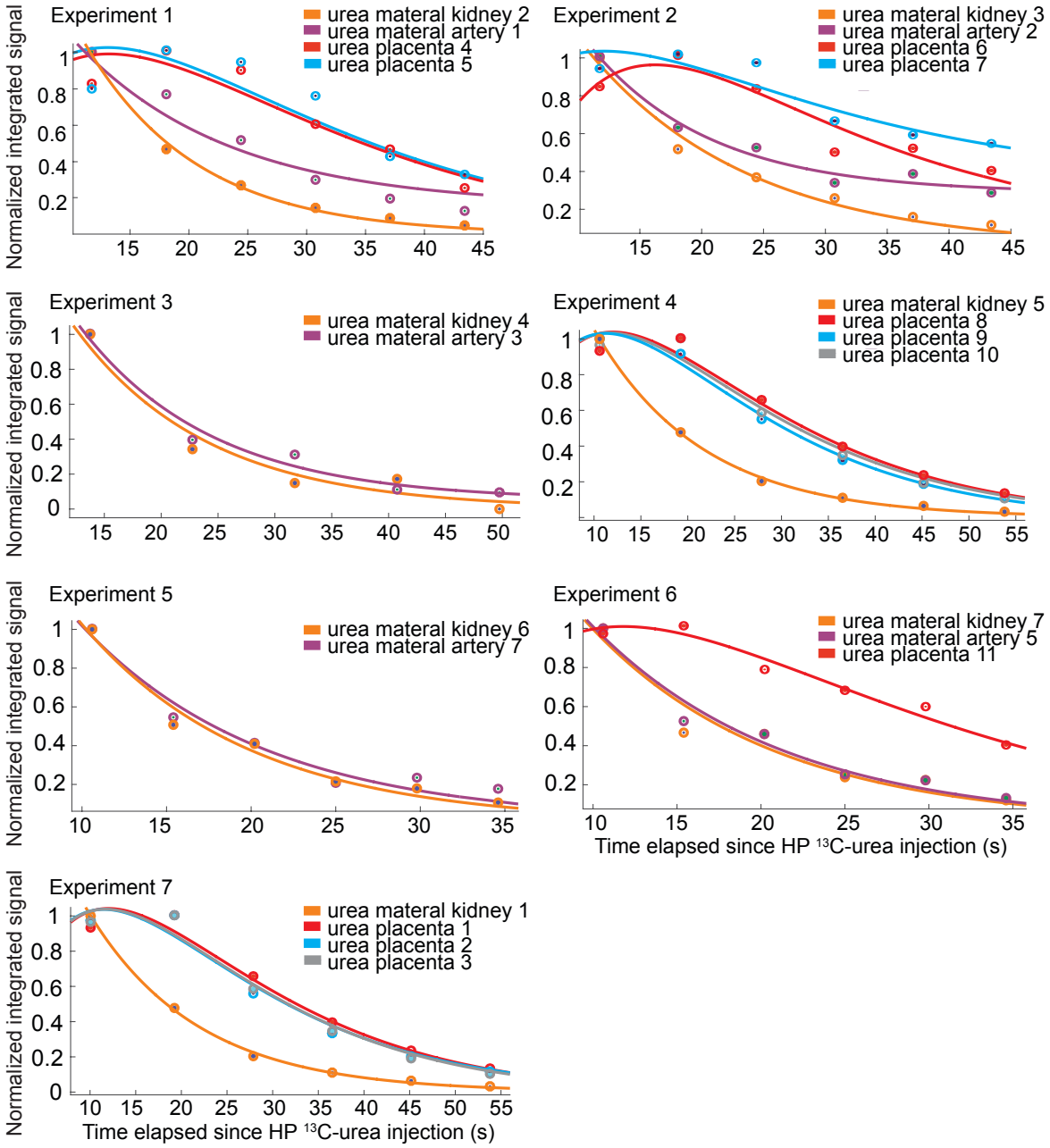

Figure S7. Best fit of the ^{13}C MRI intensities recorded as a function of time for different maternal or placental regions, after injection of HP ^{13}C-urea. Points indicate experimental data arising upon integrating a region-of-interest; continuous lines derive from Equations [S2].

Table S1. Summary of best fit T_1^{eff} (including genuine T_1 decay as well as pulsing- and outflow-derived magnetization decays) and K_{in} parameters deriving from the data in Figures S7 and S11

Targeted morphology	K_{in} (s^{-1})	T_1^{eff} (s)	Experiment #
Maternal kidney #1	-	11.9	7, Fig. S7
Maternal kidney #2	-	9.5	1, Fig. S7
Maternal kidney #3	-	13.1	2, Fig. S7
Maternal kidney #4	-	11.7	3, Fig. S7
Maternal kidney #5	-	11.5	4, Fig. S7
Maternal kidney #6	-	10	5, Fig. S7
Maternal kidney #7	-	11	6, Fig. S7
Maternal kidney l-NAME #1	-	11.5	5, Fig. S11
Maternal artery #1	-	13	1, Fig. S7
Maternal artery #2	-	9.7	2, Fig. S7
Maternal artery #3	-	11.6	3, Fig. S7
Maternal artery #4	-	10.9	5, Fig. S7
Maternal artery #5	-	11.5	6, Fig. S7
Maternal artery l-NAME #1	-	11.2	1, Fig. S11
Maternal artery l-NAME #2	-	8	2, Fig. S11
Maternal artery l-NAME #3	-	8.4	6, Fig. S11
Maternal artery l-NAME #4	-	2.4	10, Fig. S11
Placenta #1	0.10	12	7, Fig. S7
Placenta #2	0.11	11.5	7, Fig. S7
Placenta #3	0.10	11.7	7, Fig. S7
Placenta #4	0.075	13.2	1, Fig. S7
Placenta #5	0.078	13.1	1, Fig. S7
Placenta #6	0.11	11	2, Fig. S7
Placenta #7	0.080	12	2, Fig. S7
Placenta #8	0.094	12	4, Fig. S7
Placenta #9	0.10	11.2	4, Fig. S7
Placenta #10	0.095	11.7	4, Fig. S7
Placenta #11	0.092	11.8	6, Fig. S7
Placenta l-NAME #1	0.17	13.6	1, Fig. S11
Placenta l-NAME #2	-	11.8	1, Fig. S11
Placenta l-NAME #3	0.23	8.4	2, Fig. S11
Placenta l-NAME #4	0.15	13	2, Fig. S11
Placenta l-NAME #5	0.24	7.3	3, Fig. S11
Placenta l-NAME #6	0.21	8.8	3, Fig. S11
Placenta l-NAME #7	-	4.6	4, Fig. S11
Placenta l-NAME #8	0.25	6	4, Fig. S11
Placenta l-NAME #9	-	11	5, Fig. S11
Placenta l-NAME #10	-	8.2	6, Fig. S11
Placenta l-NAME #11	0.20	9.2	7, Fig. S11
Placenta l-NAME #12	-	9.1	8, Fig. S11
Placenta l-NAME #13	0.26	7	8, Fig. S11
Placenta l-NAME #14	-	12	8, Fig. S11
Placenta l-NAME #15	-	4.4	9, Fig. S11
Placenta l-NAME #16	0.092	10.7	10, Fig. S11

Supporting Information 5. Analyses of the hyperpolarized [1-^{13}C]-pyruvate kinetics.

The Pyruvate→Lactate metabolic conversion in maternal and placental compartments observed upon injecting HP [1-^{13}C]-pyruvate were modeled according to

$$\frac{d}{dt}P_m = -\frac{P_m}{T_1^p} - K_{metab1}\cdot P_m \;\; ; \frac{d}{dt}L_m = -\frac{L_m}{T_1^L} + K_{metab1}\cdot P_m$$

$$\frac{d}{dt}P_p = -\frac{P_p}{T_1^p} + K_{in}\cdot P_m - K_{metab}\cdot P_p \;\; ; \frac{d}{dt}L_p = -\frac{L_p}{T_1^L} + K_{metab}\cdot P_p \quad . \qquad \text{[S3]}$$

where the meaning of the various symbols and the assumptions underlying these first-order kinetic equations have been described in the main text. For initial conditions $P_m(0) = Pyr$, $P_p(0) = L_p(0) = L_m(0) = 0$, these coupled equations yield the solutions

$$P_m(t) = Pyr * exp\left[-\left(\frac{1}{T_1^p} + K_{metab1}\right)t\right];$$

$$P_p(t) = \frac{Pyr\cdot K_{in}}{K_{metab} - K_{metab1}}\left\{exp\left[-\left(\frac{1}{T_1^p} + K_{metab1}\right)t\right] - exp\left[-\left(\frac{1}{T_1^p} + K_{metab}\right)t\right]\right\}$$

$$L_m(t) = \frac{Pyr\cdot T_1^p\cdot T_1^L\cdot K_{metab1}}{T_1^p\cdot T_1^L\cdot K_{metab1} + T_1^L - T_1^p}\left\{exp\left[-\left(\frac{1}{T_1^p} - \frac{1}{T_1^L} + K_{metab1}\right)t\right] + exp\left(-\frac{t}{T_1^L}\right)\right\};$$

$$L_p(t) = \left\{\frac{Pyr\cdot K_{in}}{K_{metab} - K_{metab1}}\left\{-\frac{exp\left[-\left(\frac{1}{T_1^p} - \frac{1}{T_1^L} + K_{metab1}\right)t\right]}{\frac{1}{T_1^p} - \frac{1}{T_1^L} + K_{metab1}} - \frac{exp\left[-\left(\frac{1}{T_1^p} - \frac{1}{T_1^L} + K_{metab}\right)t\right]}{\frac{1}{T_1^p} - \frac{1}{T_1^L} + K_{metab}}\right\}\right.$$

$$\left. + \frac{Pyr\cdot K_{in}\left(T_1^p\cdot T_1^L\right)^2 K_{metab} exp\left(-\frac{t}{T_1^L}\right)}{\left(\left(T_1^p + T_1^L\right)\cdot T_1^L\cdot K_{metab} + T_1^p\cdot T_1^L\cdot K_{metab1} + T_1^L - T_1^p\right)\left(T_1^L - T_1^p\right) + \left(T_1^p\cdot T_1^L\right)^2 K_{metab}K_{metab1}}\right\}$$

[S4]

These equations are considerably more complex and liable to over-fitting than their urea and bicarbonate counterparts. In view of this we decided to fix the T_1^p lifetime –which again involves a number of factors that are hard to disentangle– to 28±3 s. This value is shorter than that reported *in vivo*[4] as it accounts for pulsing and outflow effects. The following plots show the best fits of the various experiments carried out in this study to determine the metabolic and transport parameters involved in these equations. These parameters are summarized for each investigated animal and compartment in Table S2.

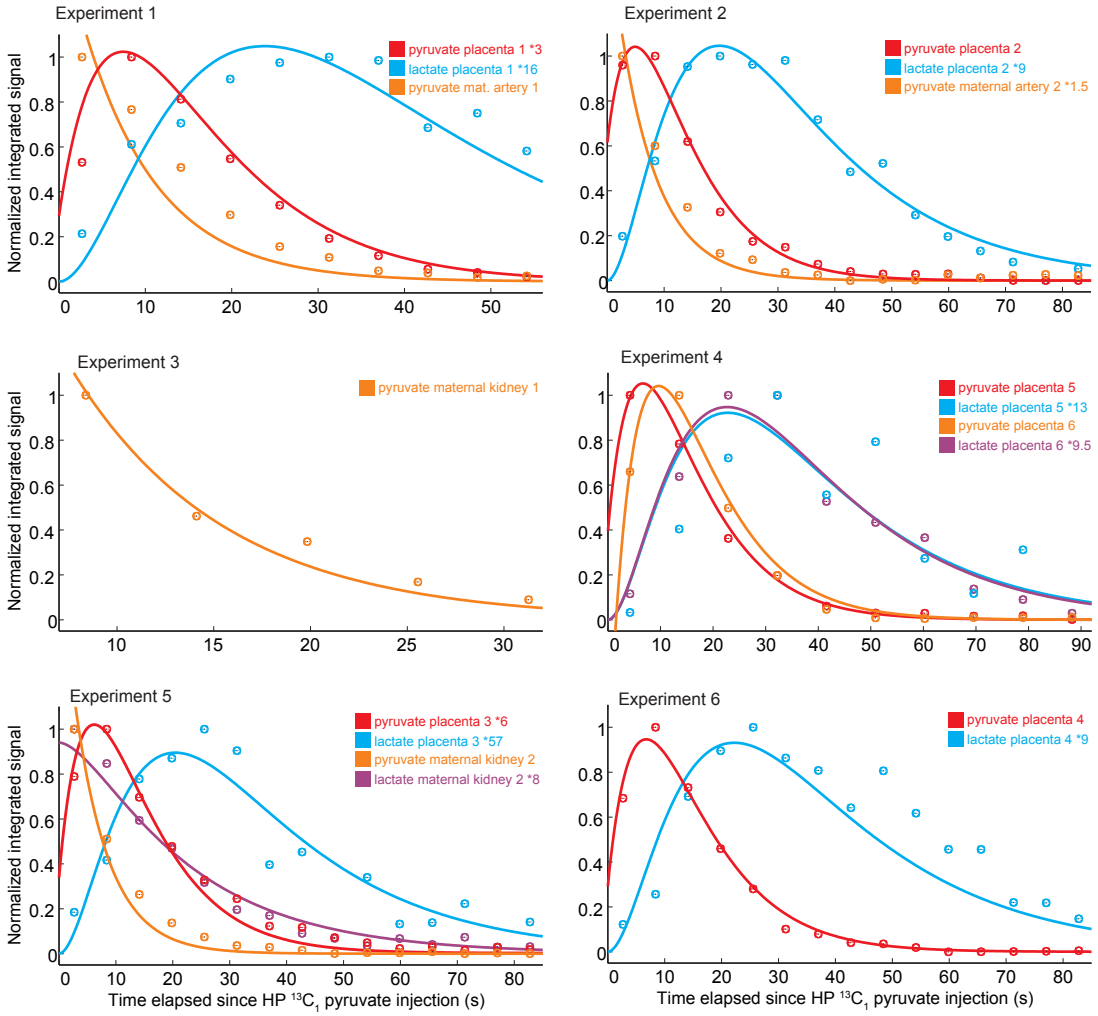

Figure S8. Best fit of the ^{13}C MRSI intensities recorded as a function of time for different maternal or placental regions, after injection of HP [1-^{13}C]pyruvate. Points indicate experimental data arising upon integrating a region-of-interest; continuous lines derive from best fits with Equations [S4].

Table S2. Summary of best fit T_1^L, T_1^p K_{in} and $K_{metab/metab1}$ parameters deriving from the data in Figures S8 and 6, to the model given by Eqs. [S4].

Targeted morphology/peak	*Pyr*	K_{in} (s^{-1})	K_{metab} (s^{-1})	T_1^L (s)	T_1^p (s)*	Experiment #
Maternal kidney #1 pyruvate	2.8	-	n.o.	-	31	3
Maternal kidney #2 pyruvate	1.8	-	0.13	-	31	5
Maternal kidney #2 lactate	1.9	-	0.15	20	-	5
Maternal artery #1 pyruvate	1.6	-	n.o.	-	31	1
Maternal artery #2 pyruvate	1.6	-	n.o.	-	31	2
Placenta #1 Pyruvate	1.6	0.21	0.080	-	25	1
Placenta #1 lactate	1.6	0.24	0.075	21	-	1
Placenta #2 pyruvate	1.6	0.25	0.10	-	25	2
Placenta #2 lactate	1.6	0.28	0.098	18	-	2
Placenta #3 pyruvate	1.9	0.20	0.080	-	31	5

Placenta #3 lactate	1.9	0.21	0.087	20	-	5
Placenta #4 pyruvate	1.9	0.18	0.084	-	27	6
Placenta #4 lactate	1.9	0.20	0.080	22	-	6
Placenta #5 pyruvate	1.9	0.20	0.07	-	31	4
Placenta #5 lactate	1.9	0.19	0.080	23	-	4
Placenta #6 pyruvate	1.9	0.19	0.085	-	25	4
Placenta #6 lactate	1.9	0.19	0.08	20	-	4
Placenta l-NAME pyruvate	1.5	0.20	0.07	-	31	Fig. 6b
Placenta l-NAME lactate	1.6	0.22	0.07	22	-	Fig. 6b

- Experiment #s refer to data sets appearing in Figure S8.
- K_{metab} refers to the Pyruvate→Lactate conversion in either the maternal or placental compartments (in the latter case corresponding to K_{metab1} in equations (S4))
- n.o. : Not observed

Supporting Information 6. Anatomical and imaging features associated to the l-NAME preeclampsia model.

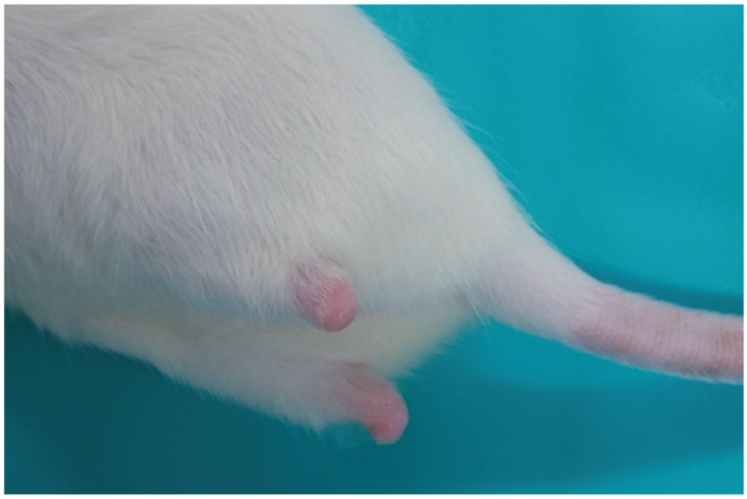

Figure S9. Truncated limbs of a recently delivered rat treated with l-NAME during pregnancy.

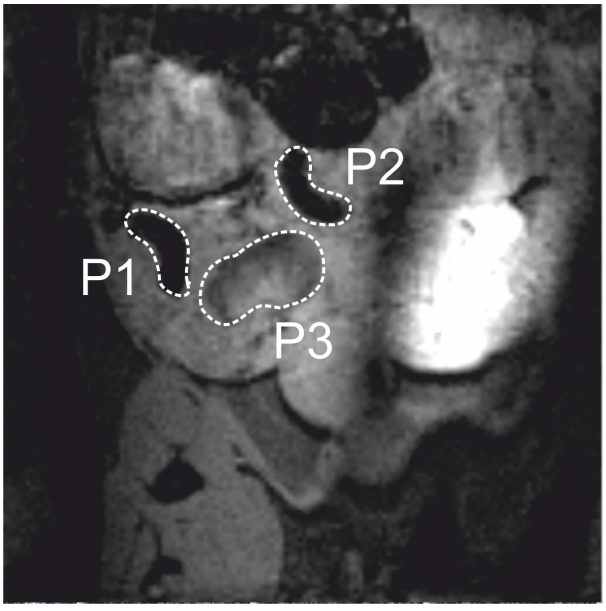

Figure S10. Anatomical proton FLASH image of a pregnant rat (E17) subject to two injections of l-NAME at 90 mg/kg/d. Highlighted by dashed lines are the dark- (P1, P2) and regular-contrast (P3) placenta.

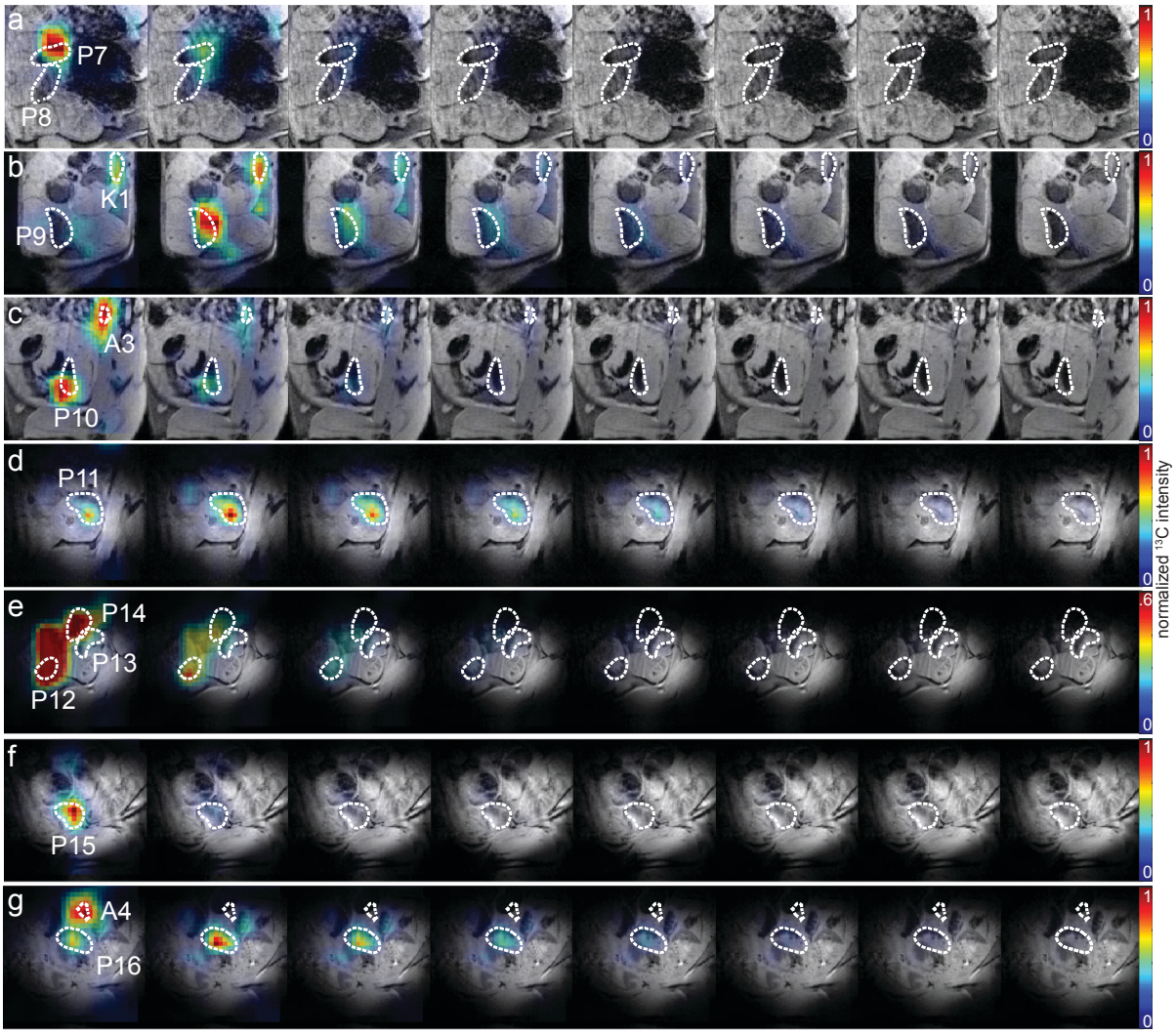

Figure S11. ^{13}C MRI experiments recorded after the injection of HP ^{13}C-urea on pregnant animals that had been pretreated with l-NAME. Dynamic ^{13}C MRSI (1.5x1.5 mm^2 in plane resolution, 5mm slice thickness) are shown overlaid on the corresponding ^{1}H MRI slices. Notice the heterogeneity in the decays of the ^{13}C-urea signal for different placentas, as well as certain misregistrations between the maximal ^{13}C enhancements and the anatomical placental units. K, maternal kidney; A, maternal artery; P, placenta.

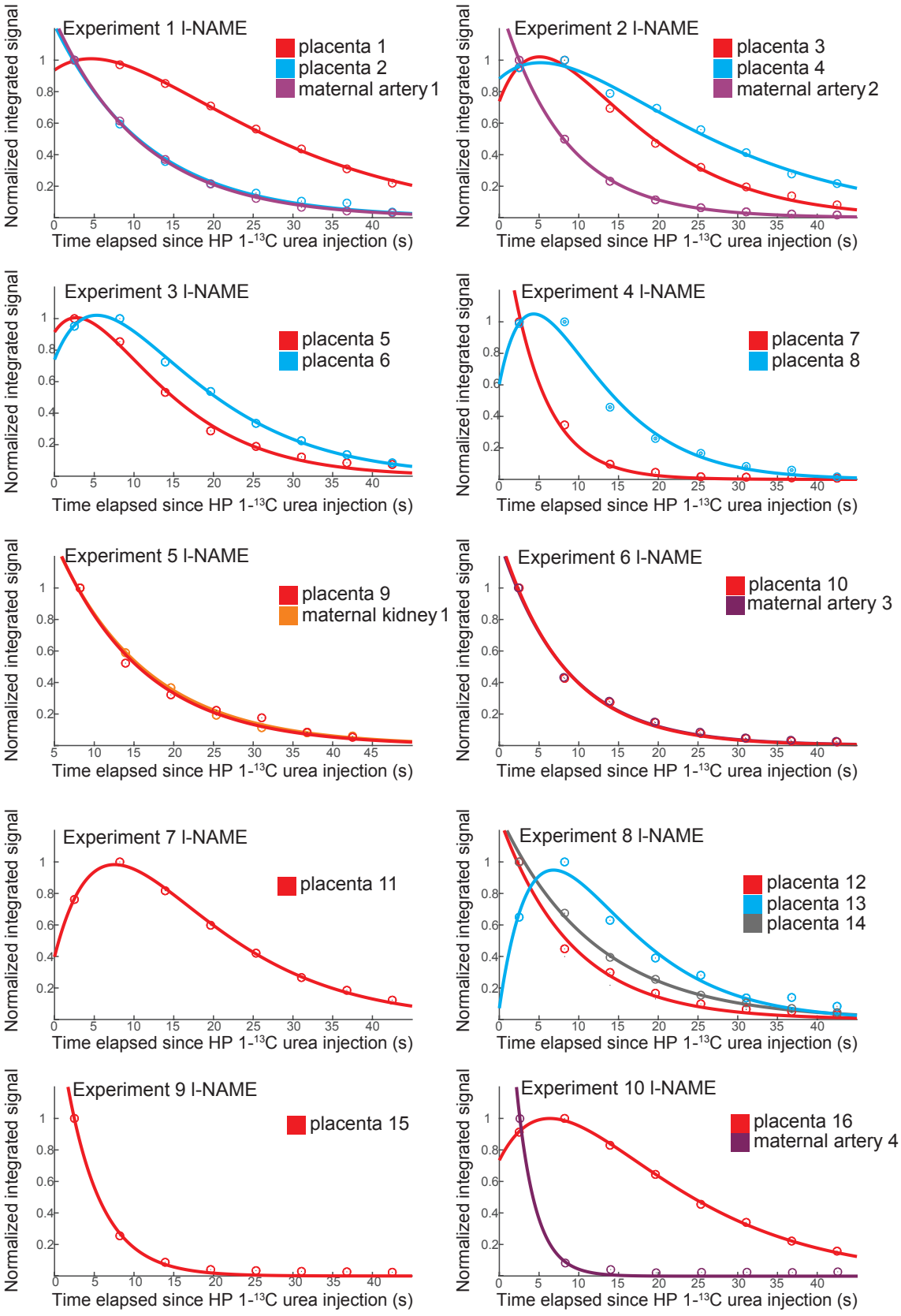

Figure S12. Best fits of the ^{13}C MRI intensities recorded as a function of time for different maternal or placental regions on the l-NAME-treated animals, after injection of HP ^{13}C-urea. Points indicate

experimental data arising upon integrating the regions-of-interest marked in Figs. 3 and S11 with similar labels; continuous lines derive from Equations [S2]. See Table S1 for details of these fits.

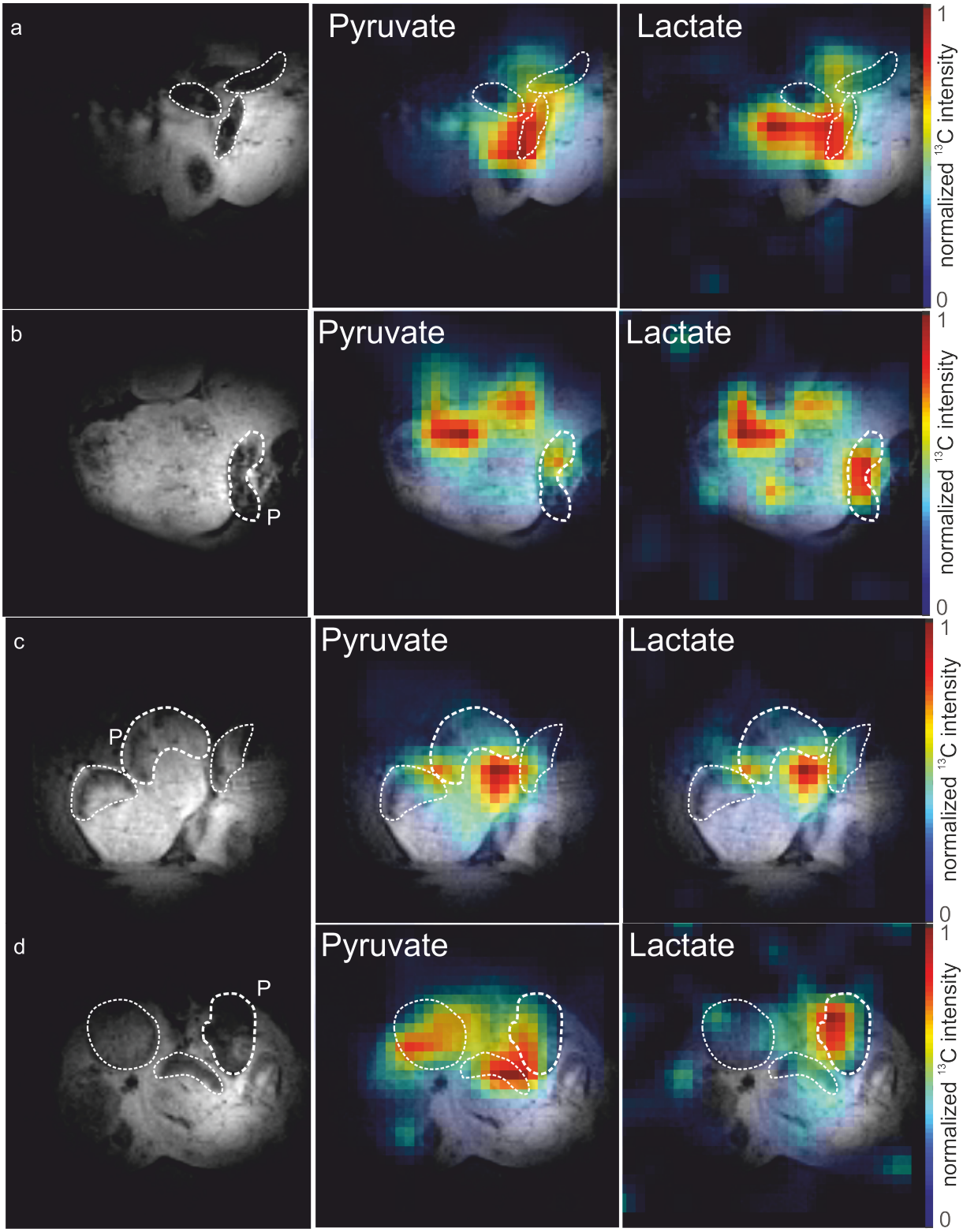

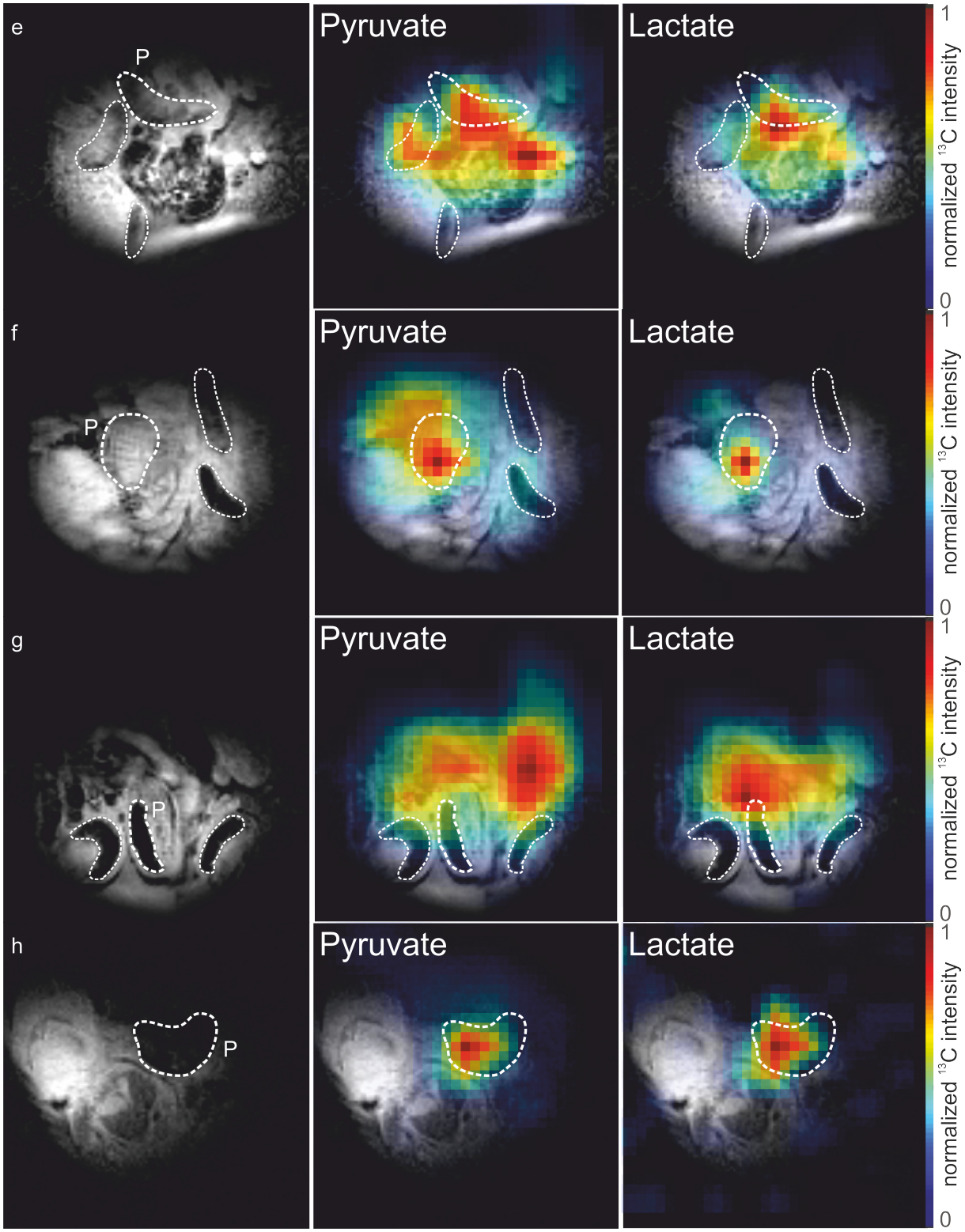
e
P
Pyruvate
Lactate
f
P
Pyruvate
Lactate
g
P
Pyruvate
Lactate
h
P
Pyruvate
Lactate
normalized ^{13}C intensity
1
0

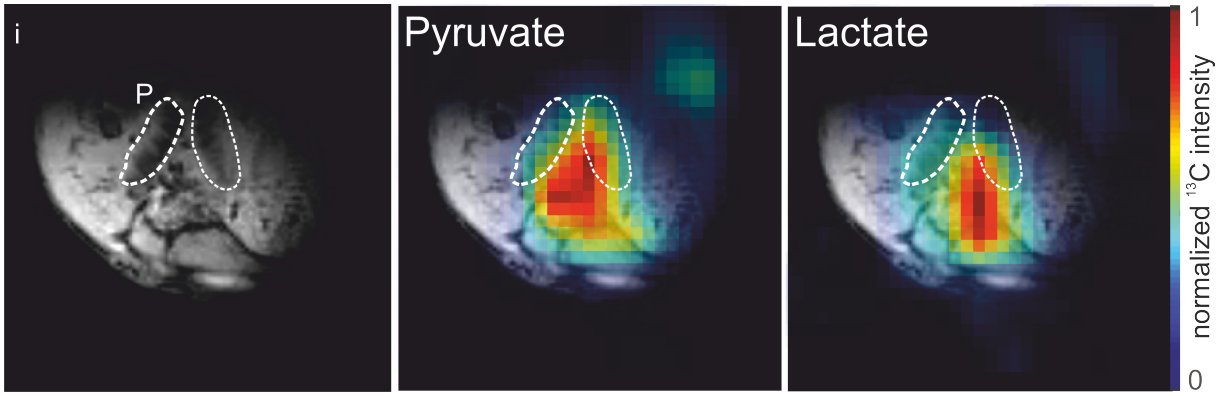

Figure S13. a-i. Localization of ^{13}C-labeled metabolites arising after injection of HP [1-^{13}C]pyruvate into rats that had been administered l-NAME. The left-hand column shows the proton anatomical images, highlighting with a P the placentas used in Figure 6c for its signal intensity analysis. The center- and right-hand columns show overlays of the [1-^{13}C]pyruvate and [1-^{13}C]lactate images arising after ca. 60 sec of signal averaging.

Supporting Information References

1. Gallagher, F. A.; Kettunen, M. I.; Day, S. E.; Hu, D. E.; Ardenkjaer-Larsen, J. H.; in't Zandt, R.; Jensen, P. R.; Karlsson, M.; Golman, K.; Lerche, M. H.; Brindle, K. M. Magnetic resonance imaging of pH in vivo using hyperpolarized (13)C-labelled bicarbonate. *Nature* **2008**, *453*, 940-U73.

2. Want, E. J.; Masson, P.; Michopoulos, F.; Wilson, I. D.; Theodoridis, G.; Plumb, R. S.; Shockcor, J.; Loftus, N.; Holmes, E.; Nicholson, J. K. Global metabolic profiling of animal and human tissues via UPLC-MS. *Nat Protoc* **2013**, *8*, 17-32.

3. Kessler A and Siekmann L. Measurement of Urea in Human Serum by Isotope Dilution Mass Spectrometry: A Reference Procedure, *Clin Chem* (1999), 45(9), 1523–1529

4. Zierhut, M. L.; Yen, Y.-F.; Chen, A. P.; Bok, R.; Albers, M. J.; Zhang, V.; Tropp, J.; Park, I.; Vigneron, D. B.; Kurhanewicz, J.; Hurd, R. E.; Nelson, S. J., Kinetic modeling of hyperpolarized (13)C-1-pyruvate metabolism in normal rats and TRAMP mice. *J Magn Reson* **2010**, *202* (1), 85-92.